



**HAL**  
open science

## Impact of the Salt Anion on K Metal Reactivity in EC/DEC Studied Using GC and XPS Analysis

Laure Caracciolo, Lénaïc Madec, Grégory Gachot, Hervé Martinez

► **To cite this version:**

Laure Caracciolo, Lénaïc Madec, Grégory Gachot, Hervé Martinez. Impact of the Salt Anion on K Metal Reactivity in EC/DEC Studied Using GC and XPS Analysis. *ACS Applied Materials & Interfaces*, 2021, 13 (48), pp.57505-57513. 10.1021/acami.1c19537 . hal-03516191

**HAL Id: hal-03516191**

**<https://univ-pau.hal.science/hal-03516191v1>**

Submitted on 9 Oct 2022

**HAL** is a multi-disciplinary open access archive for the deposit and dissemination of scientific research documents, whether they are published or not. The documents may come from teaching and research institutions in France or abroad, or from public or private research centers.

L'archive ouverte pluridisciplinaire **HAL**, est destinée au dépôt et à la diffusion de documents scientifiques de niveau recherche, publiés ou non, émanant des établissements d'enseignement et de recherche français ou étrangers, des laboratoires publics ou privés.

# Impact of the salt anion on K metal reactivity in EC:DEC studied by GC and XPS analysis.

Laure Caracciolo,<sup>a</sup> Lénaïc Madec,<sup>a,b,\*</sup> Grégory Gachot,<sup>b,c</sup> Hervé Martinez<sup>a,b</sup>

<sup>a</sup> Université de Pau et des Pays Adour, E2S UPPA, CNRS, IPREM, Pau, France

<sup>b</sup> Réseau sur le Stockage Electrochimique de l'Energie (RS2E), CNRS FR3459, 33 Rue Saint Leu, 80039 Amiens Cedex, France

<sup>c</sup> LRCS, Université de Picardie Jules Verne, 33 rue de Saint Leu, 80039 Amiens, France

\* Corresponding author: [lenaic.madec@univ-pau.fr](mailto:lenaic.madec@univ-pau.fr)

**ABSTRACT:** To develop K-ion batteries, the potassium metal reactivity in half-cell must be understood. Here it showed first that K metal leads to the migration of electrode degradation species to the working electrode surface so that half-cells SEI studies cannot be trusted. Then, the K metal reactivity was studied by combining GC/MS, GC/FTIR and XPS analysis after storage in EC:DEC wo/w 0.8M KPF<sub>6</sub> or KFSI. Comparison with Li stored in EC:DEC wo/w 0.8M LiPF<sub>6</sub> was also performed. Overall, full electrolyte degradation pathways were obtained. Results showed a similar alkali reactivity when stored in EC:DEC with the formation of CH<sub>3</sub>CH<sub>2</sub>OCO<sub>2</sub>M rich SEI. For MPF<sub>6</sub>-based electrolyte, the reactivity was driven by the PF<sub>6</sub><sup>-</sup> anion: (i) forming mostly LiF (Li metal) or (ii) catalyzing the solvent degradation into (CH<sub>2</sub>CH<sub>2</sub>COOK)<sub>2</sub> and CH<sub>3</sub>CH<sub>2</sub>COOK as main SEI products with additional C<sub>2</sub>H<sub>6</sub> release (K metal). This highlights the higher reactivity of the K system. With KFSI, the reactivity was driven by the FSI<sup>-</sup> anion degradation leading to an inorganic rich SEI. These results thus explain the better electrochemical performance often reported in half-cells with KFSI compared to KPF<sub>6</sub>. Finally, the understanding of these chemically-driven electrolyte degradation mechanisms should help researchers to design robust carbonate-based electrolyte formulations for KIBs.

## KEYWORDS

K-ion batteries, K metal reactivity, salt anion, GC/MS, GC/FTIR, XPS

## Introduction

To accelerate the energy transition from fossil fuels to renewable but intermittent energies, energy storage systems based on abundant materials such as K-ion batteries (KIBs) should be developed. Indeed, potassium abundance is about 1000 times higher than the one of Li in the earth crust. Also, in non-aqueous solvents, the low potential of the redox couple K<sup>+</sup>/K versus the other alkali metals is an advantage to develop high voltage KIBs. Moreover, high power KIBs are expected, thanks to the lowest

Lewis acidity and desolvation energy of K<sup>+</sup> compared to Na<sup>+</sup> and Li<sup>+</sup>, typically leading to higher ionic conductivity and faster electrode/electrolyte interface diffusion kinetics. Finally, inexpensive Al foil can also be chosen as a negative electrode because it does not react to form Al-K intermetallic compounds.<sup>1-3</sup>

Positive and negative electrodes studies are abundant and well documented in the literature<sup>1,4,5</sup>. However, extensive investigations of electrolytes and their reactivity remain scarce, whereas it is highly important to the battery performance. Indeed, it is well known that the quality of the solid electrolyte interphase (SEI) formed<sup>6,7</sup>, and possible gaseous products, strongly impact the cycling<sup>8</sup>. For instance, the use of KPF<sub>6</sub> (used in more than 75% of half-cell studies<sup>1</sup>) is a default choice as it leads mostly to an organic SEI with poor stability<sup>6,9-11</sup>. Indeed, inorganic SEI should be preferred because compounds such as Li<sub>2</sub>CO<sub>3</sub> and LiF bring stability to the SEI, as previously showed for Li-ion and Na-ion batteries<sup>7,12</sup>. Contrary to KPF<sub>6</sub>, inorganic-rich and stable SEI were often reported for KFSI based electrolyte with enhanced electrochemical performance.<sup>10,13-15</sup> Moreover, among the solvents used, it has been shown that the use of a linear alkyl carbonate without a co-solvent is not appropriate and that the addition of ethylene carbonate seems beneficial for electrolyte stabilization.<sup>16</sup> However, conventional 0.5-1.0M KFSI in ethylene carbonate/diethylene carbonate (EC:DEC) implies corrosion of the Al current collector starting at different potential above 3.5V as function of the salt concentration.<sup>12,17</sup>

At this point, it is important to mention that all studies described in the previous paragraph were performed in half-cells and that the impact of the highly reactive/instable K metal was neglected. This remark is of high importance because: (i) migration of electrolyte degradation products from K metal to the working electrode have been previously observed during storage of Sb half-cells and whatever the electrolyte was (1M KPF<sub>6</sub> PC, 1M KPF<sub>6</sub> PC + 5% FEC + 1% VC, 0.8M KPF<sub>6</sub> EC/DEC, 0.8M KFSI EC/DEC, 1 M KPF<sub>6</sub> DME, and 1 M KPF<sub>6</sub> diglyme).<sup>18</sup> Moreover, **Fig. 1** and **S1** shows that this phenomenon also occurs for graphite and KVPO<sub>4</sub>F half-cells, so that such interaction (also called cross-talk) between electrodes is thus driven by K metal; (ii) the coulombic efficiency (CE) of K metal plating/stripping is about 50% for conventional 0.8M KPF<sub>6</sub> EC:DEC compared to 33% for

0.8M KFSI and 99% for 0.8M or 5M KFSI DME.<sup>19</sup> This explains why KFSI DME electrolytes and especially highly concentrated ones show superior performance in half-cells.<sup>14,19-21</sup> In other words, the CE measured in half-cells is partially driven by K metal. Note that highly concentrated KFSI DME electrolytes enable the use of KFSI up to 5 V (vs K/K<sup>+</sup>) although the high salt amount may be a cost issue for the application. (iii) K metal polarization is nearly 0.1 V higher for 0.8M KFSI than for 0.8M KPF<sub>6</sub> which explains the lower rate capability generally observed with KFSI EC:DEC compared to KPF<sub>6</sub> EC:DEC, especially for negative electrodes.<sup>14</sup> Note that special care during K metal preparation can decrease its polarization and improve its stability over time.<sup>22,23</sup> In any case, electrodes capacities obtained in half-cells are thus partially driven by K metal. Overall, the use of K metal (*i.e.* the use of half-cells) misleads the interpretation of both the electrochemical performance and SEI analysis of the studied electrodes. Therefore, a better understanding of the K metal reactivity is of high importance.

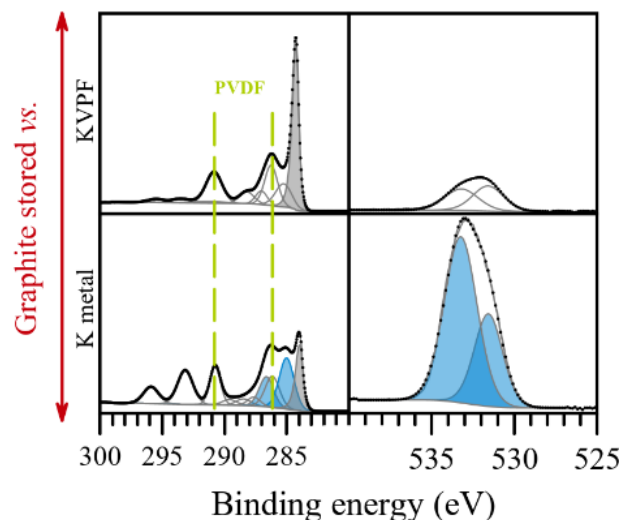


**Fig. 1** K 2p - C 1s and O 1s XPS core level spectra of graphite electrodes after 24h of storage versus either a KVPF or a potassium metal electrode using a 0.8M KPF<sub>6</sub> EC:DEC as electrolyte. Intensities were normalized for better comparison. Blue components indicate electrolyte degradation product peaks.

Thus, the present study aims at filling this gap. To understand the reactivity of K metal with the electrolyte, the method described in Fig. 2 was used: (i) K metal was stored for 3 weeks in EC:DEC solvents with or without 0.8M KPF<sub>6</sub> or 0.8M KFSI as salt, (ii) SEI formed at the metal surface was analyzed using XPS while in parallel, identification of the produced gases was performed by GC/MS and GC/FTIR, (iii) full electrolyte reaction pathways were then obtained based on lithium literature by combining produced solids (*i.e.* SEI) and gases compounds. Comparison with Li metal stored in EC:DEC or in 0.8M LiPF<sub>6</sub> EC:DEC was also performed for a better understanding.

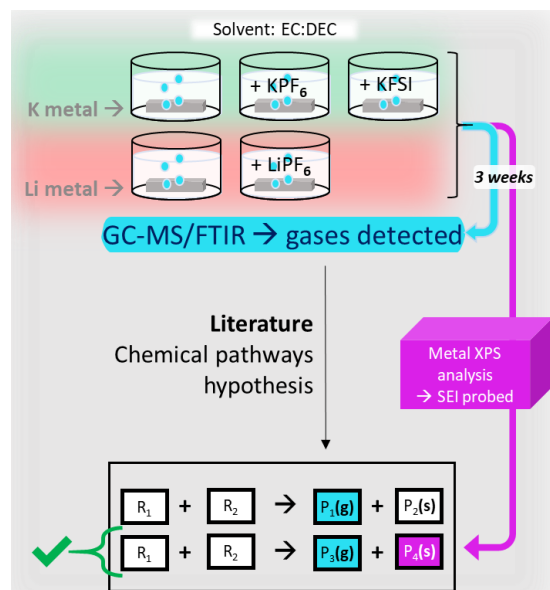


**Fig. 2** Schematic representation of the method used to study the K metal reactivity.

## Materials and methods

### Electrochemistry

**Electrolyte preparation.** 0.8M KPF<sub>6</sub>, KFSI, or LiPF<sub>6</sub> (Merck, ≥99%; Solvionic, 99.9%; Merck, 99.99%, respectively) in EC:DEC (Sigma-Aldrich, anhydrous, 99%; Sigma-Aldrich, anhydrous, ≥99%) 50:50 by volume were used as electrolytes.

**Cells preparation (interaction study).** Graphite electrodes were prepared by mixing SLP-6 graphite (Imerys Graphite & Carbon) and poly(vinylidene fluoride), PVDF (from SOLEF) with a 90:10 weight ratio, in N-methyl-2-pyrrolidone (32:68 solvent:material weight ratio), by ball-milling in an agate mortar at 500 rpm for 1h. The obtained slurry was cast on a copper current collector, dried for 24h under Ar, and finally electrodes were punch out and dried under vacuum at 80°C for 12h. KVPO<sub>4</sub>F electrodes (KVPF, carbon black and PVDF with a 85:10:5 weight ratio) were prepared following a procedure previously reported.<sup>24</sup> In an argon-filled glove box, 2032 coin cells were assembled using KVPF or graphite-based electrodes w/wo K-metal (Alfa Aesar, 99.95%), KVPF//Graphite full cells were also prepared. For all cells, a glass-fiber paper (GF/D, Whatman) and a polypropylene-polyethylene-polypropylene membrane (Celgard) were used as separators with 100 μl of 0.8M KPF<sub>6</sub> EC:DEC as electrolyte. All cells were stored for 24 hours at 25°C. After storage, coin cells were opened under argon and KVPF and graphite electrodes were washed twice by immersion during 30 s in a glass vial containing 1 ml DEC.

**Storage experiments (K metal reactivity).** K metal (Alfa Aesar, 99.95%) or Li metal (for comparison, from Goodfellow, 99.9%) electrodes with a 12mm diameter were placed on a spacer and stored in high-density polyethylene vials for 2 days, 3 weeks and 8 months in 3 mL EC:DEC solvent with or without salt (KPF<sub>6</sub>, KFSI or LiPF<sub>6</sub>), see Fig.2. After storage, K and Li electrodes were washed twice by immersion during 30 s in a glass vial containing 1 ml DEC.

### Gas chromatography

After 2 days, 22 days and 8 months, gases were collected from high-density polyethylene vials through the septum with a syringe.

**GC analysis conditions.** All analyses were performed using a trace GC ultra-gas chromatograph (Thermo Scientific). The analyzed gases were transferred into the split/splitless injector maintained at 200 °C. The chromatographic separation was performed on a “HP-PLOT/Q” polystyrene–divinylbenzene-based capillary column (30 m × 0.32 mm i.d., 20 μm) from Agilent J & W Technologies followed by a process using a post-capillary column “Rtx-1” (15 m × 0.25 mm i.d., 0.25 mm, 100% dimethyl polysiloxane) from Restek. Helium was used as the GC carrier gas and maintained at a constant flow rate of 1.3 mL min<sup>-1</sup>. To achieve the best chromatographic peaks resolution, the programmable temperature gradient was optimized from 40° to 250 °C as follows: the capillary column was ramped from the initial temperature of 40 °C, held for 6 min, increased at 10 °C/min up to 90 °C, increased at 5 °C/min up to 190 °C, held for 5 min, increased at 10 °C/min up to 250 °C, where it was held for 10min. The total duration of GC analysis was 52 min.

**FTIR conditions.** The GC was interfaced with a light-pipe GC/FTIR system (Thermo Scientific) and connected to a FTIR system Nicolet 6700 with a mid-infrared source and a medium band, liquid nitrogen cooled mercury cadmium telluride (MCT) detector. An Aldrich vapor phase FTIR library was used to identify the infrared spectra.

**MS conditions.** The GC was interfaced with an ISQ mass spectrometer (Thermo Scientific). The mass spectrometer was operated with a filament current of 250 μA, the electron energy of 70 eV in the electron ionization (EI) mode and the mass range was 10-300 u. Compound identification and corresponding structural formulae were assigned using the National Institutes of Standards (NIST) library.

### X-ray photoelectron spectroscopy

XPS analysis were performed using an Escalab 250 Xi spectrometer, with a monochromatized Al K $\alpha$  radiation (h $\nu$  = 1486.6 eV). Metal electrodes (supported by a spacer) were placed on a sample holder using uPVC insulation tape (3M part number 655), and transferred to an Ar filled glove box connected to the spectrometer. Using the standard charge compensation mode, core level spectra were recorded with a 0.15 eV step and a constant 20 eV pass energy. Using CasaXPS software, the binding energy scale was calibrated from the C-C, C-H carbon peak at 285.0 eV. This peak originates from SEI compounds and possible carbon contamination. Depending on the spectra shape, a linear or a Shirley-type background was used. 70% Gaussian - 30% Lorentzian Voigt peak shapes were selected. Full width at half-maximum and peak position constraint ranges were applied according to a previous study.<sup>18</sup> XPS quantification was performed using the relative sensitivity factor provided with the Escalab machine. Quantification values were consistent with the stoichiometry of deduced compounds and was based on a K reference compounds database previously reported by some of us.<sup>25</sup>

## Results and discussion

### Visual inspection and gas chromatography

**Fig. 3** shows the GC/MS and GC/FTIR spectra obtained for K metal (green) and Li metal (red) after storage for 3 weeks in EC:DEC, 0.8M MPF<sub>6</sub> EC:DEC and 0.8M KFSI EC:DEC as well as a summary of all gases detected and photos of metal corresponding electrodes. **Table S1** also provides a summary of the

gases detected for each system after 2 days, 3 weeks and 8 months of storage for comparison. For clarity, in the following discussion, as soon as a gas is detected, it remains detected as time goes by (see **Table S1**). For both Li and K metal stored in the EC:DEC solvents (*i.e.* without salt), CO<sub>2</sub> and C<sub>2</sub>H<sub>4</sub> gases were detected, indicating some reactivity even though no electrical current was applied. Note that these gases were already detected from 2 days of storage (**Table S1**). The color of the EC:DEC solvents remained the same, but unlike Li metal which has kept its metallic appearance, K metal has turned into a homogeneous matte purple color, thus visually indicating the passivation of its surface.<sup>26</sup> Note that no additional gases were detected after 8 months of storage.

For lithium metal stored in 0.8M LiPF<sub>6</sub> EC:DEC, neither the metal nor the electrolyte color changed after 3 weeks. On the other hand, the corresponding 0.8M KPF<sub>6</sub> EC:DEC electrolyte in contact with the potassium metal became yellow clearly indicating electrolyte degradation<sup>27</sup> while the K metal kept its original metallic appearance. Again, these results highlights the higher electrolyte reactivity with the K metal. This was further confirmed after 8 months of storage: the potassium metal totally disappeared (which was not the case for the KFSI system), indicating a full reaction of the K metal probably due to the formation of a non-stable/non-passivating SEI. Regarding the gases detected, C<sub>2</sub>H<sub>4</sub> and CO were detected for both Li and K metal stored in MPF<sub>6</sub>. Additional CO<sub>2</sub> and C<sub>2</sub>H<sub>6</sub> were detected for LiPF<sub>6</sub> and KPF<sub>6</sub> systems, respectively. After 2 days of storage, however, only CO<sub>2</sub> was detected for the LiPF<sub>6</sub> system while CO and C<sub>2</sub>H<sub>4</sub> were detected for the KPF<sub>6</sub> system (**Table S1**). Moreover, after 8 months of storage, CO<sub>2</sub> was further detected for the KPF<sub>6</sub> system (**Table S1**). Overall, these results confirm the much higher reactivity of the K metal.

For potassium metal stored in 0.8M KFSI EC:DEC, the matte purple color of the K metal also indicate the formation of a SEI. However, no gas was detected after 2 days of storage and only CO<sub>2</sub> was detected after 3 weeks while after 8 months, additional acetaldehyde was detected (**Fig. 3** and **Table S1**). Moreover, unlike K-metal in the KPF<sub>6</sub> system, the K metal electrode was still present after 8 months in the KFSI system. This result highlights the much higher reactivity of K metal and/or the formation of a more stable/passivating SEI with the KFSI salt compared to KPF<sub>6</sub> in EC:DEC, in agreement with previous studies.<sup>14</sup>

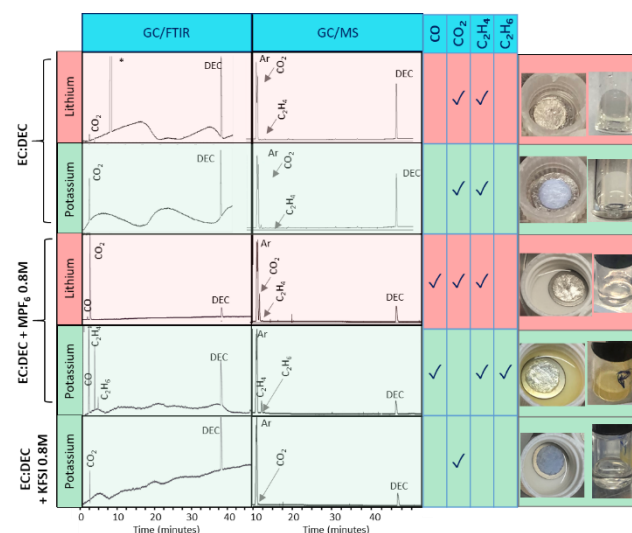


**Fig. 3** GC/MS and GC/FTIR spectra obtained after storage for 3 weeks of K metal (green) in EC:DEC, 0.8M KPF<sub>6</sub> EC:DEC and

0.8M KFSI EC:DEC. Comparison with Li metal (red) stored for 3 weeks in EC:DEC and 0.8M KPF<sub>6</sub> EC:DEC is also reported. Star signal: IR source default. A summary of all gases detected as well as photos of metal electrodes and corresponding electrolytes detected are also given.

#### XPS analysis

**Fig. 4** shows the SEI composition as obtained from XPS quantification for Li and K metal electrodes after the 3 weeks of storage in EC:DEC w/wo MPF<sub>6</sub> or KFSI salts. For clarity, **Fig. S2** shows the relevant XPS core level spectra of the corresponding electrodes while **Table S2** reports the full XPS quantification with the peaks assignment. For Li and K metal stored in EC:DEC (*i.e.* without salt), the SEI compounds detected were -(CH<sub>2</sub>CH<sub>2</sub>O)-, RCOOM, M<sub>2</sub>CO<sub>3</sub> and ROCOOM, with similar concentration, indicating similar reaction pathways. However, K metal led to a thicker SEI as no K metal was detected while Li metal accounted for about 22 at.%. This highlights the higher electrolyte reactivity with the K metal.

For Li stored in 0.8M LiPF<sub>6</sub> EC:DEC, the SEI was mainly made of LiF (~95 at.%). In the case of K metal stored in 0.8M KPF<sub>6</sub> EC:DEC, the SEI was mainly made of ROCOOK (~70 at.%) with additional -(CH<sub>2</sub>CH<sub>2</sub>O)-, RCOOK, K<sub>2</sub>CO<sub>3</sub>, KF, and other KPF<sub>6</sub> degradation products (maybe K<sub>2</sub>PO<sub>3</sub>F) in similar proportion. Note also that Li metal was still detected while K metal was not, indicating again the higher electrolyte reactivity with K metal.

For K metal stored in 0.8M KFSI EC:DEC, the SEI was made of about 60 at.% of KFSI degradation products (KSO<sub>2</sub>F, K<sub>2</sub>NSO<sub>2</sub>F, KF and FSO<sub>2</sub>NSO<sub>2</sub>) and ~35 at.% ROCOOK. Some PEO (~7at.%) was also detected.

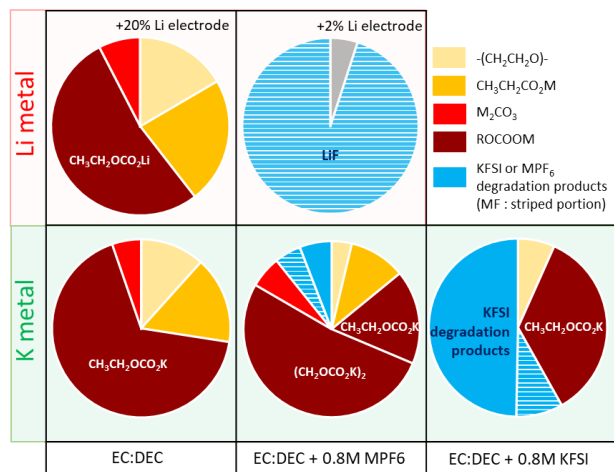


**Fig. 4** SEI composition as obtained from XPS quantification for Li- and K metal electrodes after 3 week of storage in EC:DEC, 0.8M MPF<sub>6</sub> EC:DEC and 0.8M KFSI EC:DEC. For better comparison of the SEI composition, charts exclude contribution from the metal electrode itself (indicated on the top of the chart if detected). Note that gray part for the LiPF<sub>6</sub>-based system represent unidentified products.

#### Electrolyte reactivity with K metal

**Fig. 5** gathers the possible reaction pathways involving CO, CO<sub>2</sub>, C<sub>2</sub>H<sub>4</sub> and C<sub>2</sub>H<sub>6</sub> gas detected by GC/MS, GC/FTIR (blue) as

well as ROM, RCO<sub>2</sub>M, ROCO<sub>2</sub>M, M<sub>2</sub>CO<sub>3</sub>, M<sub>2</sub>C<sub>2</sub>O<sub>4</sub>, -(CH<sub>2</sub>CH<sub>2</sub>O)-, MF and MPF<sub>6</sub> / MFSI solid detected by XPS (purple) in the case of solvents (left) and electrolytes (right) system, as reported in Li- and Na-ion literature. Degradation pathways resulting from hydrolysis are also given since traces of water have an impact on electrolyte reactivity<sup>28-31</sup>. In the following paragraphs, the K and Li metal reactivity, *i.e.* degradation pathways for EC:DEC w/wo salts are discussed based on **Fig. 5** and the GC/MS, GC/FTIR and XPS results obtained in the present study. For better clarity and direct comparison, **Fig. 6** depicts the global degradation mechanisms deduced for each system.

Considering Li and K metal stored in the EC:DEC (*i.e.* without salt), CO<sub>2</sub> could have been formed through **Eq. 03** to **Eq. 07**<sup>28,30,32-36</sup>. **Eq. 04** to **06** are, however, unlikely to happen as they occur above room temperature<sup>36,37</sup> and/or are expected to be slow<sup>33</sup>. Note that if **Eq. 07** occurred, **Eq. 28** also occurred. However, both reactions are rejected. Indeed, **Eq. 07** would require a significant amount of water/moisture<sup>38</sup> while for **Eq. 28** no MHCO<sub>3</sub> nor ethanol were detected by XPS and GC, respectively. Thus, among all CO<sub>2</sub>-releasing reactions, the most probable one is **Eq. 03**. It is proposed that upon contact, a direct electron transfer occurs from the metal electrode and the EC molecules. Considering C<sub>2</sub>H<sub>4</sub>, it could have been formed through **Eq. 08** to **10**. As XPS quantification suggests that (CH<sub>2</sub>OCO<sub>2</sub>M)<sub>2</sub> is not an SEI component (**Fig. S2** and **Table S2**), thus **Eq. 09** is excluded. Also, **Eq. 10** involves the reduction of a compound that is negatively charged twice (*i.e.* a multistep reaction starting with **Eq. 16**). Thus, the formation of C<sub>2</sub>H<sub>4</sub> more likely occurred through **Eq. 08**, *i.e.* via a 2 electrons reduction of EC also forming M<sub>2</sub>CO<sub>3</sub> as observed by XPS. Note also that **Eq. 16** could not be confirmed due to the relatively high solubility of (CH<sub>2</sub>CH<sub>2</sub>OCO<sub>2</sub>M)<sub>2</sub><sup>39</sup>. Similarly, **Eq. 14** could not be confirmed. Solid products detected by XPS could have been formed through **Eq. 15** to **Eq. 28**<sup>31,32,35,40-43</sup>. However, **Eq. 28** was excluded before while **Eq. 15**, **20**, **24** and **26** can also be excluded since no ether gas nor ethanol were detected. Moreover, **Eq. 27** is less likely to happen as it involves reducing a compound that is already twice negatively charged. As **Eq. 19** would lead to **Eq. 20**, it is thus also excluded. Accordingly, CH<sub>3</sub>CH<sub>2</sub>COOM is formed through **Eq. 25**. Also, **Eq. 17** and **23** form poly(ethylene carbonate) polymers, but the characteristic C 1s peak of ROCOOR (with R= alkyl chain) at 290.4eV<sup>44</sup> was not observed for both Li- and K-systems. Thus, even if it is possible that such compounds are soluble (especially for short polymeric chains), it is likely that **Eq. 17** and **23** didn't occur. Finally, the main SEI compound, CH<sub>3</sub>CH<sub>2</sub>OCOOM, is formed through **Eq. 22**, thus involving first **Eq. 18** and **21**. Note that this multi-step mechanism was well described in Li literature<sup>30</sup>, and also explains the -(CH<sub>2</sub>CH<sub>2</sub>O)- (*i.e.* PEO-like polymer) observed in the SEI by XPS. Overall, for K and Li stored in EC:DEC, a similar reactivity was observed (**Fig. 6**): EC first reacts with the metal to form CH<sub>3</sub>CH<sub>2</sub>OM + CO<sub>2</sub>, M<sub>2</sub>CO<sub>3</sub> + C<sub>2</sub>H<sub>4</sub> and CH<sub>3</sub>CH<sub>2</sub>COOM + CH<sub>3</sub>CH<sub>2</sub>OM (**Eq. 03**, **08** and **25**, respectively), then CH<sub>3</sub>CH<sub>2</sub>OM further reacts with EC and DEC to form CH<sub>3</sub>CH<sub>2</sub>OCOOM and PEO-like polymers (**Eq. 18**, **21** then **22**).

Considering Li and K metal stored in the 0.8M MPF<sub>6</sub> EC:DEC, completely different electrolyte degradation pathways occurred. Indeed, Li- and K-SEI are >95 at.% vs. ~10 at.% inorganic, respectively. Thus, the electrolyte reactivity for the Li system is driven by the PF<sub>6</sub><sup>-</sup> anion that forms LiF either by equilibrium with PF<sub>5</sub> (**Eq. 38**), or by hydrolysis (**Eq. 29** and **30**), or by reaction with the solvent/solvent degradation production (**Eq. 34**, **35**, **40** to **42** and **45**). Note that among **Eq. 29** to **47** (*i.e.* possible MPF<sub>6</sub> degradation pathways<sup>27,28,30,31,34,45-49</sup>), **Eq. 34** was rejected since it occurs above room temperature, and equations involving PO<sub>3</sub>,

HF, CH<sub>3</sub>CH<sub>2</sub>F and F<sub>2</sub>PO<sub>2</sub>CH<sub>2</sub>CH<sub>3</sub> (*i.e.* fluorinated liquid or gas products) could not be confirmed due to their low volatility (fluorinated liquid) or their high reactivity with the GC column (HF, POF<sub>3</sub>). Note also that M<sub>x</sub>PO<sub>y</sub>F<sub>z</sub> detected by XPS likely originates from *Eq. 42, 43, 46* and *47*. Regarding K metal stored in 0.8M KPF<sub>6</sub> EC:DEC, the electrolyte reactivity seems also driven by the PF<sub>6</sub><sup>-</sup> anion but via a catalysis of the solvent reduction. Indeed, almost no KF was detected while (CH<sub>2</sub>OCOOK)<sub>2</sub> was the main SEI product and is likely formed through *Eq. 09* with C<sub>2</sub>H<sub>4</sub> release. Moreover, C<sub>2</sub>H<sub>6</sub> (not detected for other systems) could have been formed through *Eq. 11* to *13*. Indeed, if *Eq. 13* occurred, it also involves *Eq. 18, 21* and *22*, as previously proposed for K stored in EC:DEC and it explains the formation of K<sub>2</sub>CO<sub>3</sub>, CH<sub>3</sub>CH<sub>2</sub>OCOOK and more importantly the formation of PEO-like polymers, observed in the SEI by XPS. Also, *Eq. 12* is known to be electrochemically driven<sup>30</sup> and if it occurred, *Eq. 11* could also occur, which would explain K<sub>2</sub>CO<sub>3</sub> and CH<sub>3</sub>CH<sub>2</sub>OCOOK detected by XPS. Note that CH<sub>3</sub>CH<sub>2</sub>COOK could also be formed through *Eq. 25*, as for salt-free systems. Note also that CO, detected for both Li and K stored in EC/DEC + MPF<sub>6</sub>, is likely formed through *Eq. 01* and not via *Eq. 02* because EC is considered more reactive than DEC to produce CO<sup>8</sup>. Overall, for K stored in 0.8 M KPF<sub>6</sub> EC:DEC, the PF<sub>6</sub><sup>-</sup> anion more likely catalyzes EC degradation into CO and ROM species. Finally, among *Eq. 29* to *Eq. 47, Eq. 46* and *47* could have formed the M<sub>2</sub>PO<sub>3</sub>F detected by XPS with a preferential pathway via *Eq. 46*.

Regarding K metal stored in 0.8M KFSI EC:DEC, CO<sub>2</sub> could have been formed through *Eq. 03* to *07* as well as *Eq. 28* and *29*. However, as explained previously, *Eq. 04* to *07* can also be excluded here. Moreover, *Eq. 28* and *29* involve first a large hydrolysis of the KFSI salt into HF (*Eq. 51*) that is unlikely to occur due to the low charge density of the K<sup>+</sup> cation (compared to Li<sup>+</sup>)<sup>50</sup>. Thus, *Eq. 03* is the only possible CO<sub>2</sub>-releasing reaction. Regarding CH<sub>3</sub>CH<sub>2</sub>OCOOM detected XPS, it is likely formed through the multistep reaction pathway involving *Eq. 18, 21* and *22* as discussed previously. Considering the KFSI degradation pathways, *Eq. 48* to *51* are possible but only *Eq. 48* and *49* were confirmed by XPS. Finally, the acetaldehyde detected after 8 months of storage (**Table S1**), likely forms through a slower EC decomposition into CO<sub>2</sub> + CH<sub>3</sub>-CH=O,<sup>51</sup> and/or through a poly(carbonate) reaction with ROK<sup>52</sup> (involving *Eq. 17* and/or *Eq. 23*). Overall, 0.8M KFSI EC:DEC electrolyte is the most attractive one to be used with K metal as much lower gases were detected in addition to the formation of an inorganic-rich SEI, both driven by the FSI<sup>-</sup> anion. These results can thus explain the

better electrochemical performance often reported in half-cells using KFSI salt compared to KPF<sub>6</sub>.

At this point, the experimental results (*i.e.* the electrolyte degradation pathway) obtained in this work are more likely explained by the M<sup>+</sup>-solvent (here M = Li or K) solvation structure, which is determined by the electrolyte composition (solvent chemistry, anion type and salt concentration). Indeed, recent theoretical calculation studies<sup>16,53</sup> reports that: (i) K<sup>+</sup> donates more easily an electron to the solvent than Li<sup>+</sup> for a given M<sup>+</sup>-solvent pair. Also, Li<sup>+</sup>-EC pair is the most stable one among carbonates. It thus explains the higher solvent reduction observed with K, while for Li, the PF<sub>6</sub><sup>-</sup> dissociation drives the electrolyte reactivity ; (ii) for a given M<sup>+</sup>-solvent-anion complex, the closer the anion is to the M<sup>+</sup>, the higher the stability of the solvent is. Interestingly, FSI<sup>-</sup> is found located closer to the K<sup>+</sup> than the PF<sub>6</sub><sup>-</sup>. It thus explains the higher solvent reduction observed with the PF<sub>6</sub><sup>-</sup> anion while the FSI<sup>-</sup> anion (known to be easily reduced), being close to the K<sup>+</sup>, is reduced instead of the solvent. Finally, for the given M<sup>+</sup>-EC:DEC-PF<sub>6</sub><sup>-</sup> complex, the PF<sub>6</sub><sup>-</sup> is expected to be located closer to the Li<sup>+</sup> than the K<sup>+</sup>, which would further increase the solvent reduction with K. However, such impact would need to be confirmed by further theoretical calculations.

## Conclusion

This work investigated the K and Li metal reactivity in EC:DEC with/without MPF<sub>6</sub> or KFSI salt. Interestingly, a similar solvent degradation was observed for both K and Li stored in EC:DEC without salt with the formation of CO<sub>2</sub> and C<sub>2</sub>H<sub>4</sub> gases as well as a CH<sub>3</sub>CH<sub>2</sub>OCOOM rich SEI.

The addition of an MPF<sub>6</sub> salt completely changed the reactivity: For the Li system, the degradation was driven by the PF<sub>6</sub><sup>-</sup> anion forming mostly LiF (>90 at.%). For the K system, the PF<sub>6</sub><sup>-</sup> anion catalyzed the solvent degradation with the formation of (CH<sub>2</sub>CH<sub>2</sub>OCOOK)<sub>2</sub> and CH<sub>3</sub>CH<sub>2</sub>OCOOK as main SEI products with the release of additional C<sub>2</sub>H<sub>6</sub>, thus highlighting the higher reactivity of the K system.

At the opposite, for the KFSI-based electrolyte, the reactivity was driven by the FSI<sup>-</sup> anion degradation, leading to an inorganic rich SEI.

Overall, these results can explain the better electrochemical performance often reported in half-cells using KFSI salt compared to KPF<sub>6</sub>. Finally, the understanding of these chemically-driven electrolyte degradation mechanisms should help researchers in future studies to design robust carbonate-based electrolyte formulations for KIBs.

Eq. n°	Solvent degradation products	Eq. n°	Electrolyte degradation products
01	$DEC \xrightarrow{2M^0} 2(MO) + CO$	29	$2 HF + M_2CO_3 \rightarrow H_2O(l) + 2 MF + CO_2$
02	$EC \xrightarrow{2M^0} MO + OM + CO$	30	$HF + \begin{matrix} O \\ \parallel \\ CH_3CH_2O \\   \\ OM \end{matrix} \rightarrow CH_3CH_2OH + MF + CO_2$ (liquid)
03	$EC \xrightarrow{M^0, H^+} MO + CO_2$	31	$POF_3 + DEC \rightarrow OPF_2OCH_2CH_3 + CH_3CH_2F(g) + CO_2$ (liquid)
04	$\begin{matrix} O \\ \parallel \\ MO \\   \\ OM \end{matrix} \xrightarrow{\Delta} MO + CO_2$	32	$POF_3 + EC \rightarrow OPF_2OCH_2CH_2F + CO_2$ (liquid)
05	$\left( \begin{matrix} O \\ \parallel \\ MO \\   \\ OM \end{matrix} \right)_n \xrightarrow{\Delta} \left\{ \begin{matrix} O \\ \parallel \\ MO \\   \\ OM \end{matrix} \right\}_n + n CO_2$	33	$\begin{matrix} O \\ \parallel \\ MO \\   \\ OM \end{matrix} \xrightarrow{+n(EC)} OPF_2 \left\{ \begin{matrix} O \\ \parallel \\ MO \\   \\ OM \end{matrix} \right\}_n F + CO_2$
06	$EC + H_2O \xrightarrow{\Delta} HO \begin{matrix} O \\ \parallel \\ MO \\   \\ OM \end{matrix} + CO_2$ (liquid)	34	$PF_5 + M_2CO_3 \xrightarrow{\Delta} POF_3 + 2 MF + CO_2$
07	$2 \left( \begin{matrix} O \\ \parallel \\ MO \\   \\ OM \end{matrix} \right) + H_2O(l) \rightarrow M_2CO_3 + 2 CH_3CH_2OH + CO_2$ (liquid)	35	$PF_5 + \begin{matrix} O \\ \parallel \\ MO \\   \\ OM \end{matrix} \rightarrow POF_3 + MF + CH_3CH_2F(g) + CO_2$
08	$EC \xrightarrow{2M^0} M_2CO_3 + C_2H_4$	36	$DEC + PF_5 \rightarrow C_2H_5OCOOPF_4 + HF + C_2H_4$ (liquid)
09	$2EC \xrightarrow{2M^0} \begin{matrix} O \\ \parallel \\ MO \\   \\ OM \\   \\ OM \\   \\ OM \end{matrix} + C_2H_4$	37	$OPF_2OCH_2CH_2F \rightarrow OPF_2OH + C_2H_4$ (liquid)
10	$MO \begin{matrix} O \\ \parallel \\ MO \\   \\ OM \\   \\ OM \\   \\ OM \end{matrix} \xrightarrow{2M^0} M_2C_2O_4 + MO \begin{matrix} O \\ \parallel \\ MO \\   \\ OM \end{matrix} + C_2H_4$		
11	$EC \xrightarrow{2M^0, 2H^+} M_2CO_3 + C_2H_6$		
12	$DEC \xrightarrow{M^0, H^+} \begin{matrix} O \\ \parallel \\ MO \\   \\ OM \end{matrix} + C_2H_6$		
13	$\begin{matrix} O \\ \parallel \\ MO \\   \\ OM \end{matrix} \xrightarrow{M^0, H^+} M_2CO_3 + C_2H_6$		
14	$DEC \xrightarrow{M^0, R^+} MO + \begin{matrix} O \\ \parallel \\ R \\   \\ CH_2CH_3 \end{matrix}$ (liquid)	38	$MPF_6 \rightleftharpoons PF_5 + MF$
15	$DEC + MO \rightarrow \begin{matrix} O \\ \parallel \\ MO \\   \\ OM \end{matrix} + CH_3CH_2OCH_2CH_3(g)$	39	$PF_5 + H_2O(l) \rightarrow POF_3 + 2HF$
16	$2(EC) \xrightarrow{2M^0} \begin{matrix} O \\ \parallel \\ MO \\   \\ OM \\   \\ OM \\   \\ OM \end{matrix}$	40	$PF_5 + MO \rightarrow POF_3 + MF + CH_3CH_2F(g)$
17	$n(EC) + \begin{matrix} O \\ \parallel \\ MO \\   \\ OM \end{matrix} \rightarrow \left( \begin{matrix} O \\ \parallel \\ MO \\   \\ OM \end{matrix} \right)_n \begin{matrix} O \\ \parallel \\ MO \\   \\ OM \end{matrix}$	41	$POF_3 + MO \rightarrow \begin{matrix} F \\   \\ O \\   \\ MO \end{matrix} + MF$ (liquid)
18	$EC + MO \rightarrow \begin{matrix} O \\ \parallel \\ MO \\   \\ OM \\   \\ OM \end{matrix}$	42	$POF_3 + 2n(M^0) \rightarrow n(MF) + M_nPF_{3-n}O$
19	$\begin{matrix} O \\ \parallel \\ MO \\   \\ OM \\   \\ OM \\   \\ OM \end{matrix} \xrightarrow{x2} \begin{matrix} O \\ \parallel \\ MO \\   \\ OM \\   \\ OM \\   \\ OM \\   \\ OM \end{matrix} + \begin{matrix} O \\ \parallel \\ MO \\   \\ OM \end{matrix}$	43	$MPF_6 + 2 H_2O(l) \rightarrow MPO_2F_2 + 4 HF$
20	$\begin{matrix} O \\ \parallel \\ MO \\   \\ OM \\   \\ OM \\   \\ OM \end{matrix} \rightarrow (CH_2OCH_2)_2(g) + \begin{matrix} O \\ \parallel \\ MO \\   \\ OM \end{matrix}$	44	$M_2PO_3F + H_2O(l) + MF \rightarrow M_2PO_4 + 2 HF$
21	$\begin{matrix} O \\ \parallel \\ MO \\   \\ OM \\   \\ OM \\   \\ OM \end{matrix} + DEC \rightarrow \begin{matrix} O \\ \parallel \\ MO \\   \\ OM \\   \\ OM \\   \\ OM \\   \\ OM \end{matrix} + MO$	45	$MPF_6 + 2 CH_3CH_2OH \rightarrow OPF_2OCH_2CH_2F + MF + 2HF + CH_3CH_2F(g)$ (liquid)
22	$\begin{matrix} O \\ \parallel \\ MO \\   \\ OM \\   \\ OM \\   \\ OM \end{matrix} \xrightarrow{xn} n \left( \begin{matrix} O \\ \parallel \\ MO \\   \\ OM \end{matrix} \right) + \begin{matrix} O \\ \parallel \\ MO \\   \\ OM \end{matrix}$	46	$MPO_2F_2 + MF + H_2O(l) \rightarrow M_2PO_3F + 2 HF$
23	$\begin{matrix} O \\ \parallel \\ MO \\   \\ OM \\   \\ OM \\   \\ OM \end{matrix} \xrightarrow{xn} \left( \begin{matrix} O \\ \parallel \\ MO \\   \\ OM \end{matrix} \right)_{2n} + n(MO) + DEC$	47	$MPF_6 + OPF_2OH \rightarrow MPO_2F_2 + HF + PF_5$
24	$EC \xrightarrow{M^0, R^+} \begin{matrix} O \\ \parallel \\ R \\   \\ OM \end{matrix} + CH_2OCH_2(g)$	48	$\begin{matrix} F \\   \\ O \\   \\ N \\   \\ O \\   \\ F \end{matrix} \xrightarrow{2M^0} MNSO_2 + MF + MSO_2F$
25	$EC \xrightarrow{2M^0, H^+, R^+} \begin{matrix} O \\ \parallel \\ R \\   \\ OM \end{matrix} + MO$	49	$\begin{matrix} F \\   \\ O \\   \\ N \\   \\ O \\   \\ F \end{matrix} \xrightarrow{2M^0} MF + \begin{matrix} O \\ \parallel \\ N \\   \\ O \\   \\ O \end{matrix}$
26	$2 \left( \begin{matrix} O \\ \parallel \\ MO \\   \\ OM \end{matrix} \right) \xrightarrow{M^0, H^+} MO + M_2C_2O_4 + CH_3CH_2OH$ (liquid)	50	$\begin{matrix} F \\   \\ O \\   \\ N \\   \\ O \\   \\ F \end{matrix} \xrightarrow{MO} \begin{matrix} O \\ \parallel \\ N \\   \\ O \\   \\ O \end{matrix} + 2 MF$
27	$MO \begin{matrix} O \\ \parallel \\ MO \\   \\ OM \\   \\ OM \end{matrix} \xrightarrow{2M^0} MO \begin{matrix} O \\ \parallel \\ MO \\   \\ OM \end{matrix} + M_2C_2O_4$	51	$\begin{matrix} F \\   \\ O \\   \\ N \\   \\ O \\   \\ F \end{matrix} + H_2O(l) \rightarrow \begin{matrix} O \\ \parallel \\ N \\   \\ O \\   \\ O \end{matrix} + HF$
28	$\begin{matrix} O \\ \parallel \\ MO \\   \\ OM \end{matrix} + H_2O(l) \rightarrow MHCO_3 + CH_3CH_2OH$ (liquid)		

**Fig. 5** Possible reaction pathways involving CO, CO<sub>2</sub>, C<sub>2</sub>H<sub>4</sub> and C<sub>2</sub>H<sub>6</sub> gas detected by GC/MS, GC/FTIR (blue) as well as ROM, RCO<sub>2</sub>M, ROCO<sub>2</sub>M, M<sub>2</sub>CO<sub>3</sub>, M<sub>2</sub>C<sub>2</sub>O<sub>4</sub>, -(CH<sub>2</sub>CH<sub>2</sub>O)-, MF and MPF<sub>6</sub> / MFSI solid detected by XPS (purple) in the case of solvents (left) and electrolytes (right) system, as reported in Li- and Na-ion literature. Degradation pathways resulting from hydrolysis are also given since traces of water have an impact on electrolyte reactivity. M<sup>0</sup> stands for K or Li metal (*i.e.* electron donation).

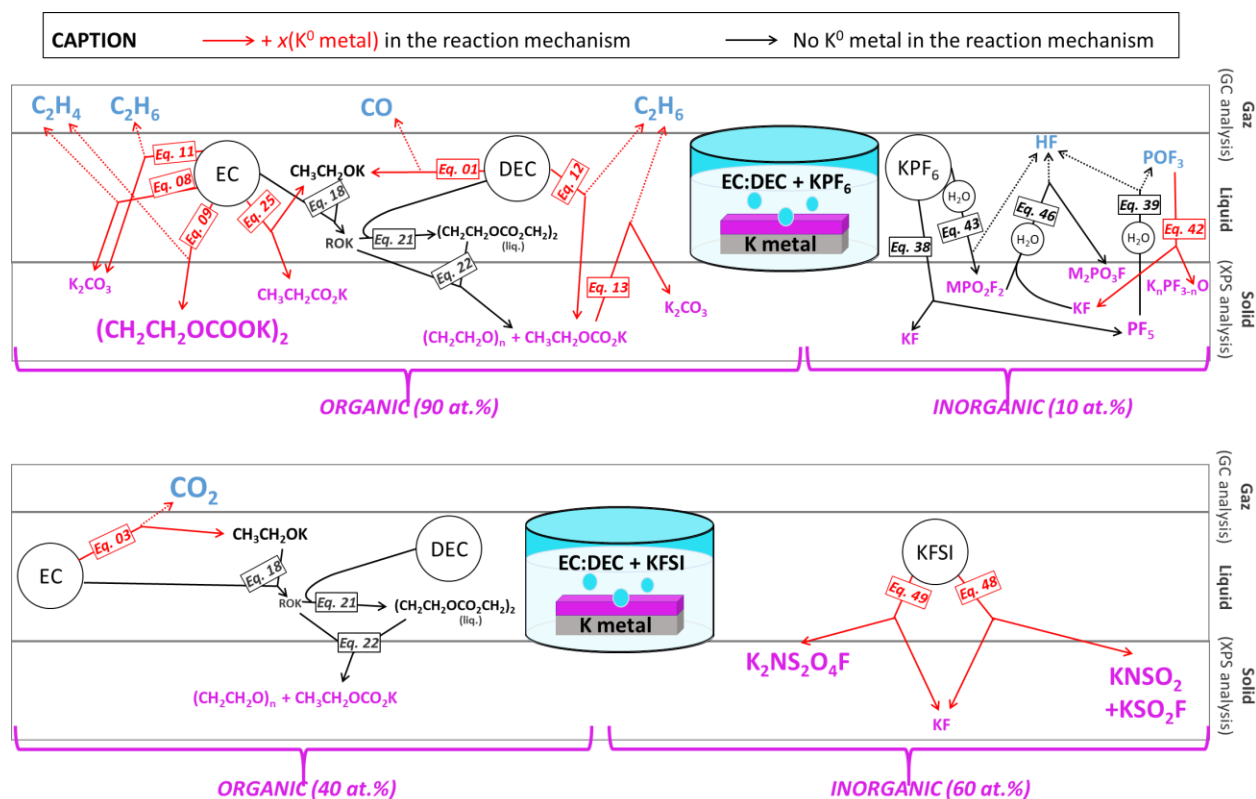


**Fig. 6** Global electrolyte degradation mechanisms for K metal stored in 0.8M KPF<sub>6</sub> (top) or KFSI (bottom) EC:DEC as deduced from GC/MS, GC/FTIR and XPS analysis. Reactions with a red arrow involves the reduction from the K<sup>0</sup> (*i.e.* electron donation from the K metal) while reactions with a black arrow are chemically driven reactions. For comparison, note that for Li metal stored in 0.8M LiPF<sub>6</sub> EC:DEC, the SEI is about 95 at.% of LiF from the PF<sub>6</sub><sup>-</sup> anion degradation.

## ASSOCIATED CONTENT

### Supporting Information

The Supporting Information is available free of charge on the ACS Publications website.

Tables including summary of gas detected by gas chromatography and quantification table from XPS analysis. Figures including XPS core level spectra of KVPF and graphite electrodes after storage in half- and full-cells, and of Li and K electrodes after storage in the different electrolytes.

### Author Contributions

All authors have given approval to the final version of the manuscript.

### Notes

The authors declare no competing financial interest.

## ACKNOWLEDGMENT

### Acknowledgments

The project leading to this publication has received funding from Excellence Initiative of Université de Pau et des Pays de

l'Adour – I-Site E2S UPPA, a French “Investissements d’Avenir” programme.

## References

- (1) Hosaka, T.; Kubota, K.; Hameed, A. S.; Komaba, S. Research Development on K-Ion Batteries. *Chem. Rev.* **2020**, *120* (14), 6358–6466. <https://doi.org/10.1021/acs.chemrev.9b00463>.
- (2) Ahmed, S. M.; Suo, G.; Wang, W. A.; Xi, K.; Iqbal, S. Bin. Improvement in Potassium Ion Batteries Electrodes: Recent Developments and Efficient Approaches. *J. Energy Chem.* **2021**, *62*, 307–337. <https://doi.org/10.1016/j.jechem.2021.03.032>.
- (3) Zhang, W.; Yin, J.; Wang, W.; Bayhan, Z.; Alshareef, H. N. Status of Rechargeable Potassium Batteries. *Nano Energy* **2021**, *83* (November 2020), 105792. <https://doi.org/10.1016/j.nanoen.2021.105792>.
- (4) Zhang, C.; Zhao, H.; Lei, Y. Recent Research Progress of Anode Materials for Potassium-Ion Batteries. *Energy Environ. Mater.* **2020**, *3* (2), 105–120. <https://doi.org/10.1002/eem2.12059>.
- (5) Zhang, L.; Wang, W. (Alex); Ma, X.; Lu, S.; Xiang, Y. Crystal, Interfacial and Morphological Control of Electrode Materials for Nonaqueous Potassium-Ion Batteries. *Nano Today* **2021**, *37*, 101074. <https://doi.org/10.1016/j.nantod.2020.101074>.
- (6) Zhang, X.; Meng, J.; Wang, X.; Xiao, Z.; Wu, P.; Mai, L. Comprehensive Insights into Electrolytes and Solid Electrolyte Interfaces in Potassium-Ion Batteries. *Energy Storage Mater.*



- 2021**, 38 (December 2020), 30–49. <https://doi.org/10.1016/j.ensm.2021.02.036>.
- (7) Peled, E.; Menkin, S. Review—SEI: Past, Present and Future. *J. Electrochem. Soc.* **2017**, *164* (7), A1703–A1719. <https://doi.org/10.1149/2.1441707jes>.
- (8) Onuki, M.; Kinoshita, S.; Sakata, Y.; Yanagidate, M.; Otake, Y.; Ue, M.; Deguchi, M. Identification of the Source of Evolved Gas in Li-Ion Batteries Using <sup>13</sup>C-Labeled Solvents. *J. Electrochem. Soc.* **2008**, *155* (11), 794–797. <https://doi.org/10.1149/1.2969947>.
- (9) Wang, H.; Wang, H.; Chen, S.; Zhang, B.; Yang, G.; Gao, P.; Liu, J.; Fan, X.; Huang, Y.; Lin, J.; Shen, Z. A Depth-Profiling Study on the Solid Electrolyte Interface: Bis(Fluorosulfonyl)Imide Anion toward Improved K<sup>+</sup> Storage. *ACS Appl. Energy Mater.* **2019**, *2* (11), 7942–7951. <https://doi.org/10.1021/acsam.9b01428>.
- (10) Deng, L.; Zhang, Y.; Wang, R.; Feng, M.; Niu, X.; Tan, L.; Zhu, Y. Influence of KPF<sub>6</sub> and KFSI on the Performance of Anode Materials for Potassium-Ion Batteries: A Case Study of MoS<sub>2</sub>. *ACS Appl. Mater. Interfaces* **2019**, *11* (25), 22449–22456. <https://doi.org/10.1021/acsami.9b06156>.
- (11) Yue Zhang, Chang Liu, Zhenrui Wu, Dan Manaig, Donald J. Freschi, Zhenbo Wang, and J. L. Enhanced Potassium Storage Performance for K-Te Batteries via Electrode Design and Electrolyte Salt Chemistry. Pdf.
- (12) Kubota, K.; Dahbi, M.; Hosaka, T.; Kumakura, S.; Komaba, S. Towards K-Ion and Na-Ion Batteries as “Beyond Li-Ion.” *Chem. Rec.* **2018**, *18* (4), 459–479. <https://doi.org/10.1002/tcr.201700057>.
- (13) Liu, S.; Mao, J.; Zhang, L.; Pang, W. K.; Du, A.; Guo, Z. Manipulating the Solvation Structure of Nonflammable Electrolyte and Interface to Enable Unprecedented Stability of Graphite Anodes beyond 2 Years for Safe Potassium-Ion Batteries. *Adv. Mater.* **2021**, *33* (1), 1–9. <https://doi.org/10.1002/adma.202006313>.
- (14) Touja, J.; Gabaudan, V.; Farina, F.; Cavaliere, S.; Caracciolo, L.; Madec, L.; Martinez, H.; Boulaoued, A.; Wallenstein, J.; Johansson, P.; Stievano, L.; Monconduit, L. Self-Supported Carbon Nanofibers as Negative Electrodes for K-Ion Batteries: Performance and Mechanism. *Electrochim. Acta* **2020**, *362*. <https://doi.org/10.1016/j.electacta.2020.137125>.
- (15) Wang, H.; Yu, D.; Wang, X.; Niu, Z.; Chen, M.; Cheng, L.; Zhou, W.; Guo, L. Electrolyte Chemistry Enables Simultaneous Stabilization of Potassium Metal and Alloying Anode for Potassium-Ion Batteries. *Angew. Chemie - Int. Ed.* **2019**, *58* (46), 16451–16455. <https://doi.org/10.1002/anie.201908607>.
- (16) Li, Q.; Cao, Z.; Wahyudi, W.; Liu, G.; Park, G. T.; Cavallo, L.; Anthopoulos, T. D.; Wang, L.; Sun, Y. K.; Alshareef, H. N.; Ming, J. Unraveling the New Role of an Ethylene Carbonate Solvation Shell in Rechargeable Metal Ion Batteries. *ACS Energy Lett.* **2021**, *6* (1), 69–78. <https://doi.org/10.1021/acsenerylett.0c02140>.
- (17) Kim, H. J.; Voronina, N.; Yashiro, H.; Myung, S. T. High-Voltage Stability in KFSI Nonaqueous Carbonate Solutions for Potassium-Ion Batteries: Current Collectors and Coin-Cell Components. *ACS Appl. Mater. Interfaces* **2020**, *12* (38), 42723–42733. <https://doi.org/10.1021/acsami.0c10471>.
- (18) Madec, L.; Gabaudan, V.; Gachot, G.; Stievano, L.; Monconduit, L.; Martinez, H. Paving the Way for K-Ion Batteries: Role of Electrolyte Reactivity through the Example of Sb-Based Electrodes. *ACS Appl. Mater. Interfaces* **2018**, *10* (40), 34116–34122. <https://doi.org/10.1021/acsami.8b08902>.
- (19) Xiao, N.; McCulloch, W. D.; Wu, Y. Reversible Dendrite-Free Potassium Plating and Stripping Electrochemistry for Potassium Secondary Batteries. *J. Am. Chem. Soc.* **2017**, *139* (28), 9475–9478. <https://doi.org/10.1021/jacs.7b04945>.
- (20) Xie, J.; Li, J.; Zhuo, W.; Mai, W. Recent Progress of Electrode Materials Cooperated with Potassium Bis(Fluorosulfonyl)Imide-Containing Electrolyte for K-Ion Batteries. *Mater. Today Adv.* **2020**, *6*, 100035. <https://doi.org/10.1016/j.mtadv.2019.100035>.
- (21) Touja, J.; Le Pham, P. N.; Louvain, N.; Monconduit, L.; Stievano, L. Effect of the Electrolyte on K-Metal Batteries. *Chem. Commun.* **2020**, *56* (93), 14673–14676. <https://doi.org/10.1039/d0cc05024e>.
- (22) Caracciolo, L.; Madec, L.; Petit, E.; Gabaudan, V.; Carlier, D.; Croguennec, L.; Martinez, H. Electrochemical Redox Processes Involved in Carbon-Coated KVPO 4 F for High Voltage K-Ion Batteries Revealed by XPS Analysis. *J. Electrochem. Soc.* **2020**, *167* (13), 130527. <https://doi.org/10.1149/1945-7111/abbb0c>.
- (23) Hosaka, T.; Muratsubaki, S.; Kubota, K.; Onuma, H.; Komaba, S. Potassium Metal as Reliable Reference Electrodes of Nonaqueous Potassium Cells. *J. Phys. Chem. Lett.* **2019**, *10* (12), 3296–3300. <https://doi.org/10.1021/acs.jpcllett.9b00711>.
- (24) Caracciolo, L.; Madec, L.; Petit, E.; Gabaudan, V.; Carlier, D.; Croguennec, L.; Martinez, H. Electrochemical Redox Processes Involved in Carbon-Coated KVPO4F for High Voltage K-Ion Batteries Revealed by XPS Analysis. *J. Electrochem. Soc.* **2020**, *167* (13), 130527 (4 p.). <https://doi.org/10.1149/1945-7111/ABBB0C>.
- (25) Caracciolo, L.; Madec, L.; Martinez, H. XPS Analysis of K-Based Reference Compounds to Allow Reliable Studies of Solid Electrolyte Interphase in K-Ion Batteries. *ACS Appl. Energy Mater.* **2021**, *00* (0), 0000–0000. <https://doi.org/10.1021/acsam.1c02400>.
- (26) Park, J.; Lee, J.; Alfaruqi, M. H.; Kwak, W. J.; Kim, J.; Hwang, J. Y. Initial Investigation and Evaluation of Potassium Metal as an Anode for Rechargeable Potassium Batteries. *J. Mater. Chem. A* **2020**, *8* (33), 16718–16737. <https://doi.org/10.1039/d0ta03562a>.
- (27) Xu, C.; Renault, S.; Ebad, M.; Wang, Z.; Björklund, E.; Guyomard, D.; Brandell, D.; Edström, K.; Gustafsson, T. LiTfD: A Highly Efficient Additive for Electrolyte Stabilization in Lithium-Ion Batteries. *Chem. Mater.* **2017**, *29* (5), 2254–2263. <https://doi.org/10.1021/acs.chemmater.6b05247>.
- (28) Han, J. G.; Kim, K.; Lee, Y.; Choi, N. S. Scavenging Materials to Stabilize LiPF<sub>6</sub>-Containing Carbonate-Based Electrolytes for Li-Ion Batteries. *Adv. Mater.* **2019**, *31* (20), 1–12. <https://doi.org/10.1002/adma.201804822>.
- (29) Tasaki, K.; Kanda, K.; Nakamura, S.; Ue, M. Decomposition of LiPF<sub>6</sub> and Stability of PF<sub>6</sub><sup>-</sup> in Li-Ion Battery Electrolytes. *J. Electrochem. Soc.* **2003**, *150* (12), A1628. <https://doi.org/10.1149/1.1622406>.
- (30) Gachot, G.; Grugeon, S.; Armand, M.; Pilard, S.; Guenot, P.; Tarascon, J. M.; Laruelle, S. Deciphering the Multi-Step Degradation Mechanisms of Carbonate-Based Electrolyte in Li Batteries. *J. Power Sources* **2008**, *178* (1), 409–421. <https://doi.org/10.1016/j.jpowsour.2007.11.110>.
- (31) Gachot, G.; Ribière, P.; Mathiron, D.; Grugeon, S.; Armand, M.; Leriche, J. B.; Pilard, S.; Laruelle, S. Gas Chromatography/Mass Spectrometry as a Suitable Tool for the Li-Ion Battery Electrolyte Degradation Mechanisms Study. *Anal. Chem.* **2011**, *83* (2), 478–485. <https://doi.org/10.1021/ac101948u>.
- (32) Shin, J.; Kim, T. H.; Lee, Y.; Cho, E. A. Key Functional Groups Defining the Formation of Si Anode Solid-Electrolyte Interphase towards High Energy Density Li-Ion Batteries. *Energy Storage Mater.* **2020**, *25* (July), 764–781. <https://doi.org/10.1016/j.ensm.2019.09.009>.
- (33) Metzger, M.; Strehle, B.; Solchenbach, S.; Gasteiger, H. A. Hydrolysis of Ethylene Carbonate with Water and Hydroxide under Battery Operating Conditions. *J. Electrochem. Soc.* **2016**, *163* (7), A1219–A1225. <https://doi.org/10.1149/2.0411607jes>.
- (34) Andersson, A. M.; Herstedt, M.; Bishop, A. G.; Edström, K. The Influence of Lithium Salt on the Interfacial Reactions Controlling the Thermal Stability of Graphite Anodes. *Electrochim. Acta* **2002**, *47* (12), 1885–1898. [https://doi.org/10.1016/S0013-4686\(02\)00044-0](https://doi.org/10.1016/S0013-4686(02)00044-0).
- (35) Petibon, R.; Rotermund, L. M.; Dahn, J. R. Evaluation of Phenyl Carbonates as Electrolyte Additives in Lithium-Ion Batteries. *J. Power Sources* **2015**, *287*, 184–195. <https://doi.org/10.1016/j.jpowsour.2015.04.012>.
- (36) Sloop, S. E.; Kerr, J. B.; Kinoshita, K. The Role of Li-Ion Battery Electrolyte Reactivity in Performance Decline and Self-Discharge. *J. Power Sources* **2003**, *119–121*, 330–337. [https://doi.org/10.1016/S0378-7753\(03\)00149-6](https://doi.org/10.1016/S0378-7753(03)00149-6).

- (37) Xu, K.; Zhuang, G. V.; Allen, J. L.; Lee, U.; Zhang, S. S.; Ross, P. N.; Jow, T. R. Syntheses and Characterization of Lithium Alkyl Mono- and Bicarbonates as Components of Surface Films in Li-Ion Batteries. *J. Phys. Chem. B* **2006**, *110* (15), 7708–7719. <https://doi.org/10.1021/jp0601522>.
- (38) Heiskanen, S. K.; Kim, J.; Lucht, B. L. Generation and Evolution of the Solid Electrolyte Interphase of Lithium-Ion Batteries. *Joule* **2019**, *3* (10), 2322–2333. <https://doi.org/10.1016/j.joule.2019.08.018>.
- (39) Wang, Y.; Nakamura, S.; Ue, M.; Balbuena, P. B. Theoretical Studies To Understand Surface Chemistry on Carbon Anodes for Lithium-Ion Batteries: Reduction Mechanisms of Ethylene Carbonate. **2001**. <https://doi.org/10.1021/ja0164529>.
- (40) Gachot, G.; Grugeon, S.; Eshetu, G. G.; Mathiron, D.; Ribière, P.; Armand, M.; Laruelle, S. Thermal Behaviour of the Lithiated-Graphite/Electrolyte Interface through GC/MS Analysis. *Electrochim. Acta* **2012**, *83*, 402–409. <https://doi.org/10.1016/j.electacta.2012.08.016>.
- (41) Zhuang, G. V.; Yang, H.; Blizanac, B.; Ross, P. N. A Study of Electrochemical Reduction of Ethylene and Propylene Carbonate Electrolytes on Graphite Using ATR-FTIR Spectroscopy. *Electrochem. Solid-State Lett.* **2005**, *8* (9). <https://doi.org/10.1149/1.1979327>.
- (42) Shkrob, I. A.; Zhu, Y.; Marin, T. W.; Abraham, D. Reduction of Carbonate Electrolytes and the Formation of Solid-Electrolyte Interface (SEI) in Lithium-Ion Batteries. 1. Spectroscopic Observations of Radical Intermediates Generated in One-Electron Reduction of Carbonates. *J. Phys. Chem. C* **2013**, *117* (38), 19255–19269. <https://doi.org/10.1021/jp406274e>.
- (43) Zhuang, G. V.; Yang, H.; Ross, P. N.; Xu, K.; Jow, T. R. Lithium Methyl Carbonate as a Reaction Product of Metallic Lithium and Dimethyl Carbonate. *Electrochem. Solid-State Lett.* **2006**, *9* (2), 64–68. <https://doi.org/10.1149/1.2142157>.
- (44) Beamson, G.; Briggs, D. High Resolution XPS of Organic Polymers: The Scienta ESCA300 Database. *J. Chem. Educ.* **1993**, *70* (1), A25. <https://doi.org/10.1021/ed070pA25.5>.
- (45) Eshetu, G. G.; Grugeon, S.; Gachot, G.; Mathiron, D.; Armand, M.; Laruelle, S. LiFSI vs. LiPF<sub>6</sub> Electrolytes in Contact with Lithiated Graphite: Comparing Thermal Stabilities and Identification of Specific SEI-Reinforcing Additives. *Electrochim. Acta* **2013**, *102*, 133–141. <https://doi.org/10.1016/j.electacta.2013.03.171>.
- (46) Herstedt, M.; Abraham, D.P.; Kerr, J.B.; Edström, K. X-Ray Photoelectron Spectroscopy of Negative Electrodes from High-Power Lithium-Ion Cells. *Electrochimica Acta*, **2004**, *49* (28), 5097–5110. <https://doi.org/10.1016/j.electacta.2004.06.021>
- (47) Guéguen, A.; Streich, D.; He, M.; Mendez, M.; Chesneau, F. F.; Novák, P.; Berg, E. J. Decomposition of LiPF<sub>6</sub> in High Energy Lithium-Ion Batteries Studied with Online Electrochemical Mass Spectrometry. *J. Electrochem. Soc.* **2016**, *163* (6), A1095–A1100. <https://doi.org/10.1149/2.0981606jes>.
- (48) Li, Q.; Liu, X.; Han, X.; Xiang, Y.; Zhong, G.; Wang, J.; Zheng, B.; Zhou, J.; Yang, Y. Identification of the Solid Electrolyte Interface on the Si/C Composite Anode with FEC as the Additive. *ACS Appl. Mater. Interfaces* **2019**, *11* (15), 14066–14075. <https://doi.org/10.1021/acsami.8b22221>.
- (49) Solchenbach, S.; Metzger, M.; Egawa, M.; Beyer, H.; Gasteiger, H. A. Quantification of PF<sub>3</sub> and POF<sub>3</sub> from Side Reactions of LiPF<sub>6</sub> in Li-Ion Batteries. *J. Electrochem. Soc.* **2018**, *165* (13), A3022–A3028. <https://doi.org/10.1149/2.0481813jes>.
- (50) Reber, D.; Figi, R.; Kühnel, R. S.; Battaglia, C. Stability of Aqueous Electrolytes Based on LiFSI and NaFSI. *Electrochim. Acta* **2019**, *321*, 134644. <https://doi.org/10.1016/j.electacta.2019.134644>.
- (51) Fuhst, M. R.; Siegel, D. J. Gas Evolution in Li-Ion Batteries: Modeling Ethylene Carbonate Decomposition on LiCoO<sub>2</sub> in the Presence of Surface Magnetism. *J. Phys. Chem. C* **2020**, *124* (44), 24097–24104. <https://doi.org/10.1021/acs.jpcc.0c07550>.
- (52) Lee, J. C.; Litt, M. H. Ring-Opening Polymerization of Ethylene Carbonate and Depolymerization of Poly(Ethylene Oxide-Co-Ethylene Carbonate). *Macromolecules* **2000**, *33* (5), 1618–1627. <https://doi.org/10.1021/ma9914321>.
- (53) Zhang, J.; Cao, Z.; Zhou, L.; Park, G.-T.; Cavallo, L.; Wang, L.;

Alshareef, H. N.; Sun, Y.-K.; Ming, J.; Model-Based Design of Stable Electrolytes for Potassium Ion Batteries. *ACS Energy Letters* **2020**, *5*, 3124–313.

TOC

